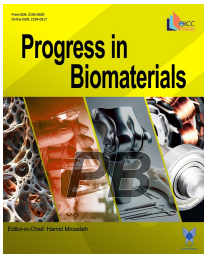

Volume 12, Issue 4, 122320 (1-11)

Progress in Biomaterials (PIBM)

https://doi.org/10.57647/pibm.2023.122320

Construction and Characterization Of a 3D Scaffold Containing 30B Modified Clay Nanoparticles for Bone Tissue Engineering

Nikoo Yazdani Elahabadi[1], Shahrokh Shojaei[1,*], Vahabodin Goodarzi[2]

[1]*Department of Biomedical Engineering, CT.C., Islamic Azad University, Tehran, Iran.*
[2]*Applied Biotechnology Research Center, Baqiyatallah University of Medical Sciences, Tehran, Iran.*

[*]**Corresponding author:** shahrokhshojaei@iau.ir

Original Research

Received:
7 August 2023
Revised:
5 November 2023
Accepted:
8 November 2023
Published online:
30 December 2023

Abstract:

This study designs and evaluates 3D scaffolding using biodegradable polymers of polylactic acid, polycaprolactone, hydroxyapatite, and 30B clay to address bone problems.
X-ray diffraction is employed to examine the crystal structure properties of the samples and the phase of the diffraction plates. The morphological study of the surfaces of samples is conducted with a field-emitting electron microscope (FESEM). The elemental analysis map test is utilized to examine the elements in the compound structures. Cell viability and toxicity are evaluated using the MTT method on the growth and reproduction of human-class MG-63 bone cells, as well as skin fibroblast cells.
An analysis of the Fourier transform infrared spectroscopy shows that the interactions between ingredients can be identified roughly based on their functional groups. Results demonstrate that the scaffolding containing all four materials has an average porosity size of 8.40 µm and a standard deviation of the diameter of the porosities of 6.31 µm. The volume percentage of porosities is 24.93%.
It can be concluded that the composition of all four materials forms a completely porous structure that can benefit the final properties of the production scaffolding. The scaffold has sufficient mechanical properties to maintain the structure of damaged bone and facilitates the formation of small pores using the salt leaching process. DAPI coloring is used to check the decellularization and core residue, showing favorable behavior.

Keywords: 3D scaffolding; 30B clay nanoparticles; Hydroxyapatite; Polycaprolactone; Polylactic acid

Cite this article: Yazdani Elahabadi, N., Shojaei, S., Goodarzi, V. Construction and Characterization Of a 3D Scaffold Containing 30B Modified Clay Nanoparticles for Bone Tissue Engineering. *Progress in Biomaterials* **12**(4), Article 20 (2023).

1. Introduction

Disturbance or loss of bone tissue can cause mobility issues. Tissue engineering can help mend injuries and fractures in the bone tissue. Various biomaterials and scaffolds have been tested for rigid tissue regeneration. However, polymers remain the most highly used biomaterials in enhancing scaffolding due to their mechanical properties and degradation rates similar to proteins in hard and soft tissues. Synthetic polymeric materials have many advantages in bone grafting because their physical properties can be tailored to their use, and their composition can be modified. The excellent flexural stability and biocompatibility of synthetic materials have gained considerable popularity in bone tissue engineering Javid-Naderi et al., 2023. The scaffold has sufficient pore volume to facilitate the transport of nutrients and wastes required for cellular betterment, migration, and proliferation. Many polymers and nanocomposites are used in regenerative medicine. Among various synthetic polymers, polyacid (PLA) and poly (σ-caprolactone) PCL have been approved by the FDA Park et al., 2017. Polyesterlactic acid and polycaprolactone are biodegradable. Polycaprolactone is hydrophobic and more crystalline than polyic acid, resulting in a reduced rate of polycaprolactone degradation. PLA has a higher stiffness and a different degradation

mechanism than PCL. The degradation mechanism of PLA involves chain scission and subsequent fragmentation, while the degradation of PCL is due to the scission of the terminal groups of the polymer chains Yao et al., 2017.

Carbajal et al. investigated scaffolding made with hydroxyapatite (HAp), polylactic acid (PLA), and commercial polycaprolactone (PCL). Overall results indicated that scaffolds with these compounds benefit from satisfactory superficial and thermal properties Torre et al., 2021.

Murugesan et al. cross-examined copolymer/clay nanocomposites for biomedical applications. Copolymers incorporated with nano clay have properties such as barrier function, rigidity, thermal/flame resistance, super hydrophobic, biocompatibility, stimulant response, continuous drug secretion, hydrolysis resistance, remarkable dynamic mechanical properties, including low-temperature flexibility and resilience, outstanding hydrolytic stability, and antimicrobial properties. The modification of the nano clay surface has provided additional properties due to improved adhesion between the polymer matrix and the clay Nano-clay, high surface free energy, and a high degree of interference or peeling morphology. The process of polymer/clay composites also has great potential for biomedical applications offering different indications, especially in drug delivery systems and regenerative medicine Murugesan and Scheibel, 2020.

Kundu et al. examined polycaprolactone (PCL) fibers mineralized with HAp MMT-clay and MMT-clay in situ using a pressurized rotation adjustment (PG) and successfully produced HAp-nano clay-PCL fibers. Built-in 3D scaffolding was able to increment bone growth, cell viability, and proliferation. The results showed that polymer fiber scaffoldings are biocompatible and that cells can grow and differentiate in fiber scaffolding Kundu et al., 2021.

Nguyen et al. obtained uniform rod-shaped SiO_2 NPs of similar sizes to bone minerals (length 17 ± 113 nm and width 7.7 ± 49 nm) by hydrothermal method using 1.3 g of CTAB. 3D biomimetic CS/SiO_2 scaffolding was successfully synthesized by solvent casting along with the salt washing technique using SiO_2 NPs as an inorganic component. SiO_2 scaffolding showed an average size of suitable pores and cavities, from 198 µm 198 to 269 µm 269 and 70.99% to 73.23%, respectively. Their results confirmed that CS/SiO_2 scaffolding could support the migration, growth, and distribution of cells when used as bone scaffolding Nga et al., 2023.

In another study, Hassanajili et al. utilized polylactic acid/polycaprolactone/hydroxyapatite (PLA/PCL/HA) composites with an indirect 3D printing method to develop bone scaffolding. In their experiment, they observed that composite scaffolding has favorable conditions such as cell survival on the scaffolding biocompatibility, optimal mechanical properties, and proper surface characteristics Hassanajili et al., 2019. Bone fractures continue to present significant challenges and require less risky treatments.

The salt leaching technique is commonly used due to its simplicity, lower cost, and better control over micro and nano structures. This method can aid in producing porous scaffolds with good mechanical properties and high specific surface area, which may be less achievable in 3D printing and electrospinning.

2. Materials and methods

2.1 Materials

All materials are laboratory-grade and have a purity of 99%. Polylactic acid polymer (200 g), hydroxyapatite nanoparticles (10 g), and clay 30B (10 g) were purchased from Sigma Aldrich (USA). All ingredients, including Polycaprolactone 200 g, dioxane solvent, 10% DMSO (CATNO:BP231-100), and DMF solvent (one liter each), as well as Hexamethylene diisocyanate HDI250CC, Polycarbazol (200 g), PEO polyethylene oxide (100 g), and $FeCl_3 \cdot 6H_2O$ (200 g) were purchased from Merck (Germany) (Table 1). We have obtained MG_63 cells and skin fibroblasts from the Pasteur Institute, with MG_63 cells identified as ATCC CRL_1427 (NCBI Code C555) and skin fibroblasts from circumcision identified as C163.

Table 1. The utilized devices and materials.

Number	Country	Manufacturer	Latin name	Material/Device description
1	Netherlands	PHILIPS company		X-ray diffraction (XRD)
2	Czech republic	TESCAN company	FESEM	Field emission scanning electron microscopy
3	USA	Thermo company	FTIR	Fourier-transform infrared spectroscopy
4	USA	BIOSERA	DMEM	Cultivation environment
5	USA	GIBCO	FBS	Fetal bovine serum
6	Germany	Sigma	Trypsin	Tricin
7	Germany	Merck	DMEM	Ethylenediaminetetraacetic acid
8	Germany	Call Roth	MTT	Tetrazolium dye
9	Iran	Kavoosh Mega	Autoclave	Autoclave
10	Germany	Hettich	Centrifuge	Centrifuge
11	Iran		Laminar hood	Hood laminase
12	Germany	BINDER	Incubator	Incubator
13	Iran		Nitrogen tanks	Nitrogen tank
14	USA	LABOMED	Light Microscope	Optical microscope
15	USA	Bio Tek	Elisa Reader	Spectrophotometer

2.1.1 Preparation of scaffolds

In this study, polymer materials must first be dissolved in their suitable solvent. The PCL granules in the DMF solvent were dissolved at 65 °C for 3 h and the PLA granules in the dioxane solvent were dissolved at room temperature for 2 h, then these two solutions were mixed and placed under intense stirring for 2 h at 50 °C. Afterward, some salt was poured into this solution and stirred well. All the salt particles were coated into our polymer material. Then, the material was poured into special molds and dried at room temperature for 1 week. The samples were then removed from the mold and placed in distilled water. Their salt particles were washed, and the samples were dried and prepared for the relevant tests. To make nanocomposite samples, we first dispersed the nanoparticles in DMF and dioxane solvents for 10 min via an ultrasonic device, allowing the polymer material to be dissolved. The rest of the work was done similarly Haider et al., 2020 (figures 1 a and b).

2.1.2 Scaffolding specifications

Infrared spectroscopy (FTIR) method was utilized to identify factor groups and chemical bonds on five samples. The articles were used to analyze the FTIR data, and its chart was drawn with Origin Pro 2022 v9.9.0.225 SR1 software. X-ray diffraction is a non-destructive method that provides comprehensive information about the chemical compounds and crystal structure of natural and industrial materials and was conducted on all five samples. The analysis was conducted using XRD data, Xpert high Sore Plus (version 5.2), and its diagram was drawn with Origin software.

The surface characteristics and morphology of the samples were examined using the field emission electron microscope (Fe-SEM) test, and all five samples were illustrated with magnifications of 200, 100, and 50. Image processing software J (version 1.50) was used to analyze Fesem.
To examine the elements in the structure of the compounds, the elemental analysis map test for the elements Si, Ca, and P was used in three samples: PLA/PCL/CLAY 30B, PLA/PCL/HA, and PLA/PCL/CLAY 30B/HA.

2.1.3 Cell proliferation

The MTT test was performed on MG-63 human bone cells and skin fibroblast on four PLA/PCL/CLAY 30B, PLA, PLA/PCL/HA, and PLA/PCL/CLAY 30B/HA samples. MG_63 cells are recognized as a suitable model for studying biological interactions and responses to biological scaffolds. One challenge may relate to these cells' ability to adapt to new scaffolds and how they can grow under various conditions.
MTT test on human bone cells: MTT was tested with a concentration of 5 mg/mL in PBS. First, the scaffolding was placed in the culture media, and approximately 5,000 cells were cultivated on the scaffolding in the 96 well plates three times and in three dimensions. To check the toxicity of the scaffolding, the plate was placed in the incubator for 24 hours, and then the conditioned media was removed.
The test was carried out by adding 100 µL of MTT solution with a dilution of 1/10 of the initial stock to each house. The plates were then incubated for 3 to 4 h at a temperature of 37 °C. After adding this solution, the color of the environment

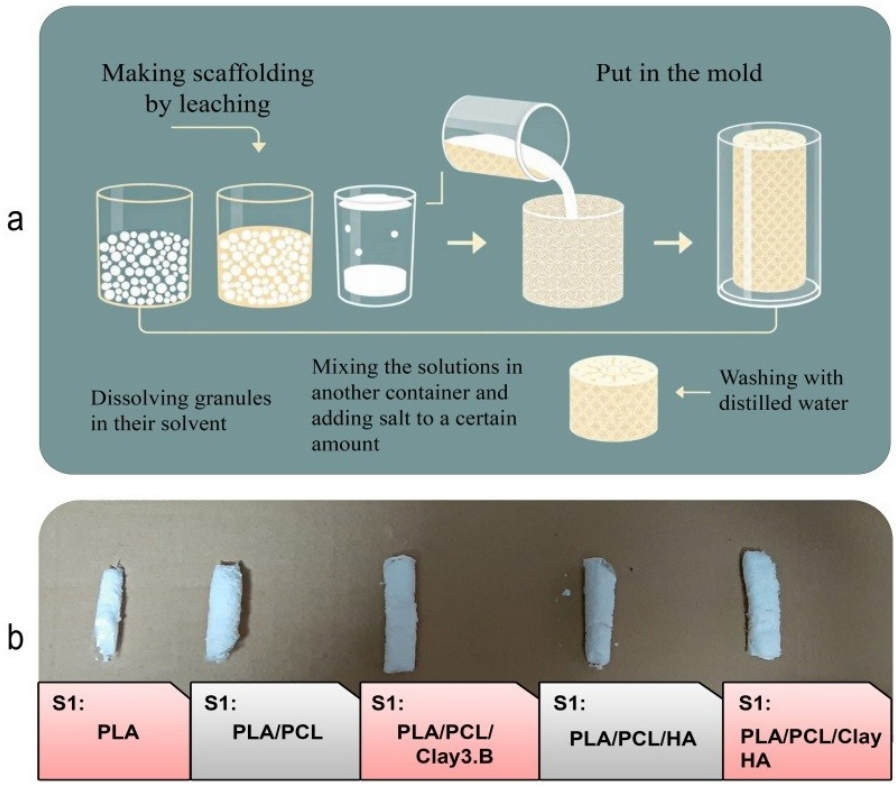

Figure 1. Construction stages (a), samples (b).

turned purple-blue due to the production of formazan. After this time, the top solution of the cell was removed, and 100 mL of DMSO was added to each house to dissolve the produced crystals. Then, they were incubated for 15 min in the incubator. After this time, the scaffolding was removed from the environment, all the plated houses were piped, and the absorption rate was measured at a wavelength of 570 nm utilizing a spectrophotometric device Ghanbari et al., 2021; Hashemi and al., 2020.

MTT test on skin fibroblast the cell class in the culture medium DMEM contains 10 percent of the fetal bovine serum, L-glutamine, and penicillin-streptomycin at 37 °C in the atmosphere containing 5% incubated carbon dioxide. After passage and cell proliferation, cell counting was conducted using Neubauer lam, and cells were transported to 48 wells with MTT scaffolding with a concentration of 5 mg/mL in PBS. First, the scaffolding was placed in the culture medium, and about 5,000 cells were cultivated on the scaffolding in the 96 well plates three times and in three dimensions. To check the toxicity of the scaffolding, the plate was placed in the incubator for 24 hours, and the conditioned medium was removed. Then, 50000 cells were moved into each plate house. A row of cultivation mediums was also intended as control, and the plates were kept for 24 and 72 hours at a temperature of 37 °C. After emptying the wells from the culture medium, 100 microliters of MTT solution were added to each well. After 3 to 4 hours, 100 µL of DMSO was added to each well to dissolve the available Fumarazen. In the last stage of optical absorption, Fumarazan was read at $570-630$ nm using the epoch reader Ayran et al., 2022.

Coloring DAPI First, the cells were fixed in 4% paraformaldehyde and then rinsed with PBS. API (Sigma-D9542) was then added with a concentration of 1 µg/ML. After 20 min, the sample was rinsed with PBS, and the photographing was conducted with a fluorescent microscope (Olympus) Hashemi and al., 2020.

3. Results and discussion

3.1 Characteristic of 3D scaffolding

Observations of chemical interaction qualitative measurements were employed in functional groups and chemical interactions within all components of each compound (Fig. 2 a).

In the FTIR spectrum, corresponding to the PLA sample, the wide peak visible in the wave number about 3495 cm^{-1} corresponds to the tensile vibrations of hydroxyl groups or the water absorbed superficially into the structure Roshanghias et al., 2022; Mohan et al., 2017.

The peaks in the number of waves about 2946 cm^{-1} and 2997 cm^{-1} corresponded to symmetrical and asymmetric tensile vibrations of C-H bonds in the methyl and methylene structures present in the PLA structure, respectively Li et al., 2018; Arunraj et al., 2019. The peak in the wave number of about 1759 cm^{-1} also corresponded to the tensile vibrations of the C=O bonds present in the carbonyl groups in the PLA Sri Aprilia et al., 2017; Evans et al., 2019. The peak also appears in the 1568 cm^{-1} wave number corresponding to the bending vibration of the O-H bond on the surface of the absorbed water Friné et al., 2019.

In addition, the couriers located in the range of wave numbers 1380 cm^{-1} to 1460 cm^{-1} were relevant to the bending vibrations of C-H in the PLA structure Nasrin et al., 2017. The couriers located in the range of wave numbers from 1000 cm^{-1} to 1200 cm^{-1} corresponded to the tensile vibrations of carbon-oxygen bonds such as C-O-C and C-OH bonds Roshanghias et al., 2022; Abo-Elseoud et al., 2018. $C\text{-}CH_3$ tensile Rocking vibration and Wagging vibration C-H links in PLA structure are shown in the number of wave numbers from 870 cm^{-1}, 756 cm^{-1}, and 688 cm^{-1} gravitational peak, respectively Jung et al., 2018. Also, the Courier corresponding to the bending vibration C=O is located at the wave number about 515 cm^{-1} Nandiyanto et al., 2019. In the PLA/PCL spectrum, PLA-related couriers are again visible, but several new PCL-related couriers also appeared in this spectrum. The new peak located at the wave number of 2867 cm^{-1} corresponds to the symmetrical tensile vibration of the C-H bonds present in the PCL structure Ardekani-Zadeh and Hosseini, 2019. The new couriers located in the 958 cm^{-1} and 454 cm^{-1} wavelengths also corresponded to the tensile vibration of the O=C-O bond and the bending vibration of the C=O bond in the PCL structure, respectively Gokalp et al., 2016; Islam and al., 2015. The presence of these peaks confirms the presence of PCL in this composite. It should be noted that some other PCL couriers, such as those relevant to the bending

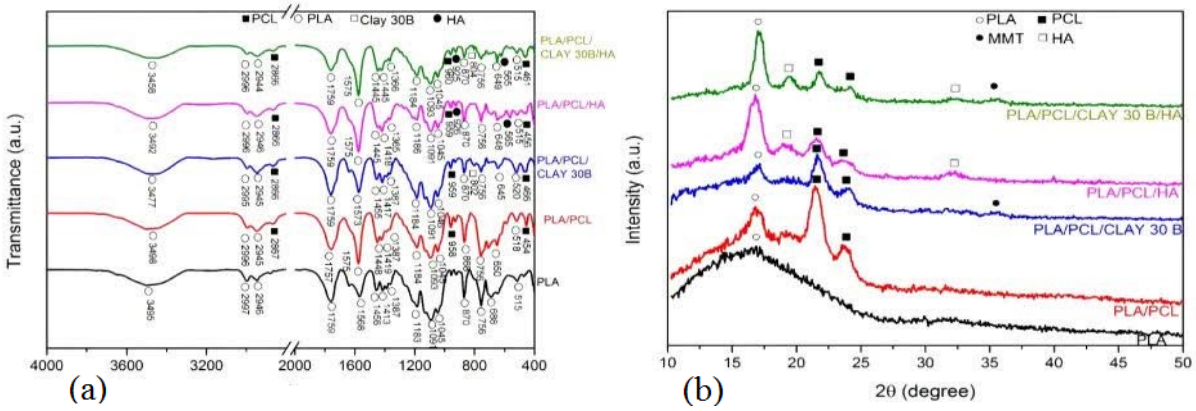

Figure 2. FT-IR spectra related to the samples examined (a), XRD results in samples (b).

and tensile vibrations of C-H and the C-O and C=O traction vibrations, overlapped with couriers related to these same vibrations in the PLA. In the sample containing clay 30b, in addition to the PLA and PCL couriers, a new courier appeared in 802 cm^{-1}, which is in line with the findings of similar articles on the bending vibration of Si-O-Si bonds in the structure of this material Contri et al., 2020; Somderama et al., 2019. Some other couriers in this structure, such as couriers related to the tensile vibration of the Si-O-Si links, overlapped with the courier related to the tensile vibration of the C-O links in PLA and PCL and, therefore, cannot be separated Wang et al., 2022. In the sample containing hydroxyapatite, in addition to the PLA and PCL couriers, a new courier appeared in 926 cm^{-1} and another in 565 cm^{-1}, corresponding to the tensile and bending vibrations of the bonds in PO4-3 in the structure of this material Tang et al., 2015; Mtavangu et al., 2022. As can be observed, in the composite sample containing all four materials (PLA, PCL, clay 30B, and HA), the corresponding couriers of all four structures have emerged.

Analysis of the XRD test: As shown in Fig. 2 b, in the PLA sample, a wide peak is visible at an angle of about 17 degrees, which has also been reported by similar articles Nasrin et al., 2017; Perumal et al., 2017; Sun et al., 2014. This peak is related to polylactic acid structures in the form α. In the PLA/PCL sample, two sharp peaks visible at angles of 21.4 and 24.5 degrees, found in similar articles Solechan et al., 2022; Hsieh et al., 2020, are related to the diffraction of plates 110 and 200 in the Orthorhombic crystal structure of the PCL, respectively. In the PLA and PCL mix samples, the peaks for both structures are again visible, but the width of the PLA-related peak has decreased. However, its intensity has increased, indicating an increase in the crystallization degree of the structure in the mixed sample compared to the pure sample. Equation (1) can be used to measure the degree of crystallization Sun et al., 2014.

$$X_c = 100 \times \frac{A_c}{A_c + A_a} \tag{1}$$

X_c is the degree of crystallization, and A_c and A_a are the subcurved surfaces in the crystalline and amorphous regions, respectively. The degree of crystallization for pure PLA and PLA-PCL samples was obtained using this relationship as 18.21% and 38.32%, respectively. After enhancing the degree of crystallization by mixing PCL and PLA formerly developed by Levitt et al. Luyt and Gasmi, 2016 and Liu et al. Liu et al., 2020 with the addition of Clay 30B to the PLA-PCL mix structure, a new weak peak was observed at about 35.6 degrees in addition to the relevant couriers to PLA and PCL, which is related to the montmorillonite structure contained in this material Fil et al., 2014. In this sample, the crystallization degree decreased to 22.31% due to the placement of clay nanoparticles between the polymer chains PLA and PCL. Also, in the diffraction pattern corresponding to the sample containing hydroxyapatite, in addition to the PCL and PLA couriers, couriers have been observed at angles of 18.9 and 32.0 degrees corresponding to the diffraction from the plates 110 and 211 of the crystal structure of hydroxyapatite, respectively (with reference code JCPDS NO. 09-0432 and the hexagonal crystal structure and the P63/m Space Group) Choe et al., 2010; Choudhary et al., 2015. The composite from these three materials has the highest crystalline degree among the materials examined due to the hydroxyapatite structure with a high crystalline degree and its proper diffusion in the PCL-PLA structure, and its crystalline degree has reached 49.8%. In the sample containing PCL-PLA with both hydroxyapatite and clay 30b, in addition to the PCL and PLA-related couriers, the courier relevant to montmorillonite is visible at an angle of about 35.6 degrees, and the couriers relevant to hydroxyapatite at angles of about 19 and 32 degrees. This proved the success of compositing between these four materials in this sample. This sample obtained a crystalline degree of 47.5%, indicating the proper diffusion of clay 30B and hydroxyapatite in the PCL-PLA structure. However, the presence of clay 30b again reduced the crystallization of this material slightly compared to the PLA/PCL/HA sample.

Microstructure observations: The FESEM analysis was employed to examine the microstructure of the samples examined from the FE-SEM test, and the resulting micrographs are shown in figures 3 a to e. The image processing software J was used to measure the volume percentage of pores in the structure and the diameter of the micro-pores. In the PLA sample, pores with dimensions of 8 to 18 µm are noticeable in the structure, with an average size of 5.21 µm and a standard deviation of 4.17 µm. This large standard deviation from the average size indicates that the porosities had highly scattered sizes and were far from the average value. The volume of porosity in this sample was 14.24%. Adding PCL to the PLA structure resulted in a significant reduction in the number of disruptions and defects in the structure, as well as a reduction in their size between 0.2 and 10 µm. In this sample, the average size and standard deviation of the diameter of the structural pores are 4.13 and 2.92 µm, respectively. The percentage of porosity volume also decreased significantly to 6.28%. Therefore, the presence of PCL in PLA increased structural density, and the porosity was obtained with sizes approximate to the average value with a narrow size distribution. Adding clay 30B to this composite resulted in the sample becoming completely porous again and the number and size of pores increasing significantly. In this sample, the average size and standard deviation of the diameter of the pores are 7.90 and 6.66 µm, respectively, and the volume percentage of the pores is 15.24%. In the sample containing hydroxyapatite, despite the greater porosity of the structure than the PLA/PCL sample, the size of the porosities was much smaller, and their volume percentage was also much lower than in the PLA/PCL/CLAY 30B sample. In this sample, the average size and standard deviation of the diameter of the pores are 4.05 and 2.49 micrometers, respectively, and the volume percentage of the pores is 8.17%.

In the sample containing all four compounds, the volume, number, and size of the cavities grew larger and reached their highest value. In this sample, the average size and standard deviation of the diameter of the pores are 8.40 and 6.3 µm 1, respectively, and the volume percentage of the pores is 24.93%. This shows that the composition of all four materials creates a completely porous structure, which can

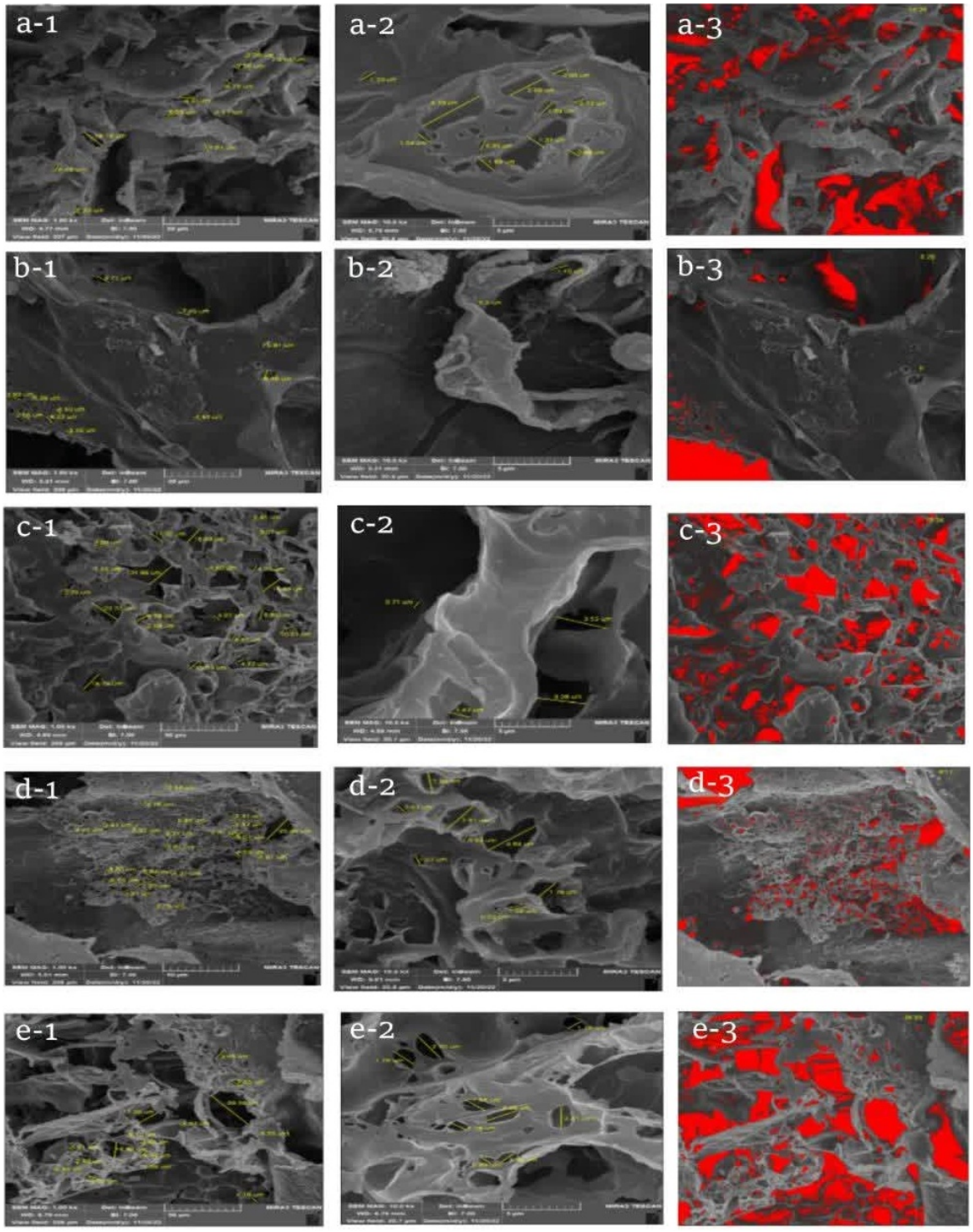

Figure 3. Micrographs of various samples ((a) PLA, (b) PLA/PCL, (c) PLA/PCL/CLAY 30B, (d) PLA/PCL/HA, and (e) PLA/PCL/CLAY 30B/HA) are presented at magnifications of 10,000× and 1,000×, including software-processed images for pore volume measurement at 1,000×.

benefit the final properties of the production scaffolding.

3.1.1 Dispersion of nanoparticles

The elemental analysis map test was utilized for PLA/PCL/-CLAY 30B, PLA/PCL/HA, and PLA/PCL/CLAY 30B/HA samples to examine the elements in the structure of the compounds, and the results are shown in figures 4 a to c. figure 4 a shows that SI elements also exist in a significant form in the structure of the material, indicating the presence of the clay 30B structure in this sample. The presence of CA elements is also due to the presence of impurities in the clay 30B compound. It can be seen that all elements are distributed optimally throughout the material, indicating the proper distribution of clay 30b in PLA/PCL composites. In figure 4 b, elements such as P and Ca are identified in the structure of the material, indicating the presence of hydroxyapatite structure in this sample. As can be observed, all elements are distributed optimally throughout the mate-

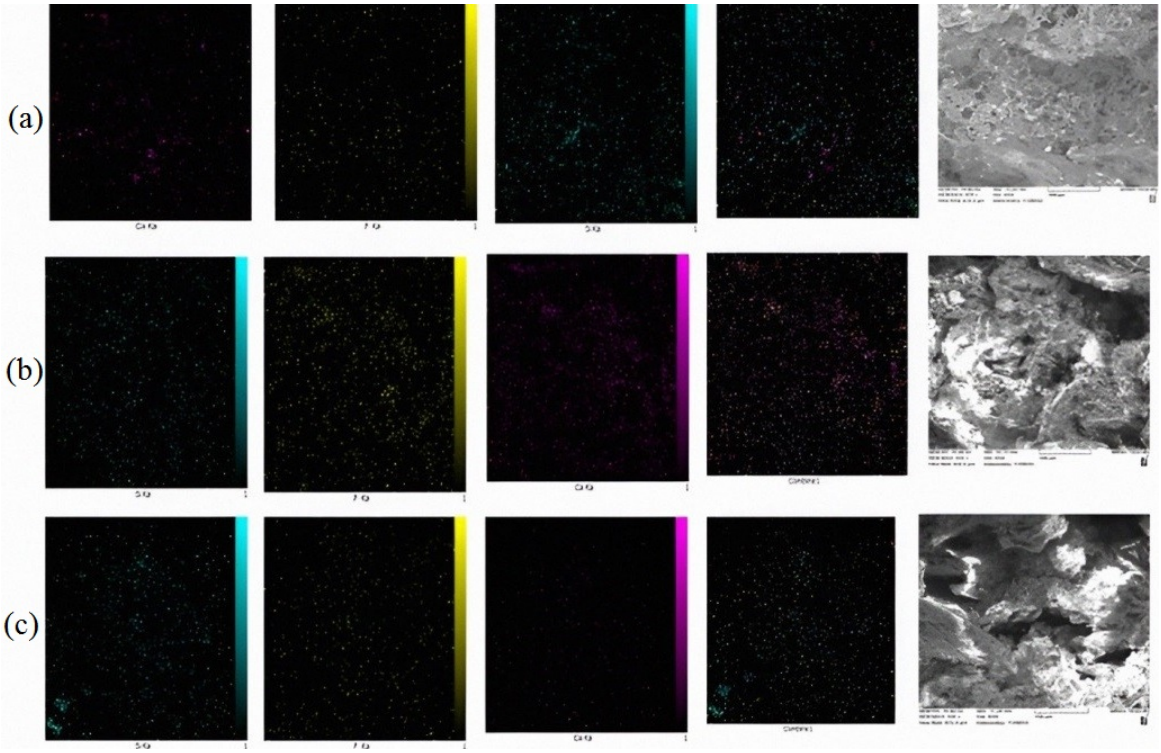

Figure 4. Elemental mapping analysis results are presented for the (a) PLA/PCL/CLAY 30B, (b) PLA/PCL/HA, and (c) PLA/PCL/CLAY 30B/HA samples.

rial, indicating the proper distribution of hydroxyapatite in PLA/PCL composites.

Finally, in the PLA/PCL/CLAY 30B/HA composite sample, Si, Ca, and P elements have been identified, indicating the simultaneous presence of clay 30B and HA in this sample. All elements are distributed optimally throughout the material in this composite, indicating the proper distribution of hydroxyapatite and clay 30B in PLA/PCL composites Kareem et al., 2019.

4. Biological testing

4.1 MTT analysis

Spectrophotometric data analysis and determination of cell survival on human class bone cells: The cell color began to change after the addition of the DMSO. The control samples were cultured. They were completely purple, showing that the cells were alive. But higher mortality rate was associated with a whiter color of the well. Finally, the optical absorption of the solution obtained at a wavelength of 570 Nm was read by the spectrophotometer device, and the percentage of cell survival was calculated using the following formula (equation (2)).

$$\text{percentage of survival of each treatment sample} = \frac{\text{control sample absorption}}{\text{treatment sample absorption}} \times 100 \quad (2)$$

The groups were designed as follows and incubated for 24 h in an incubator at a temperature of 37 °C.

According to the control group and the graph of other samples, the cells survived on each scaffolding, and all scaffoldings displayed adequate compatibility (figure 5).

The combination of polylactic acid, polycaprolactone, hydroxyapatite, and clay and cell viability: Although there is evidence of the toxicity of clay particles, this may be because the concentration of clay particles in the final composition is low enough that their toxic effects are diminished. Furthermore, chemical interactions between the different components of the composition may reduce negative effects and maintain cell viability.

The results of the 24-and 72-h cell toxicity tests of the scaffolding on the fibroblast cell line of the skin showed that the scaffolding had no toxicity on the fibroblast cells. The growth rate of skin fibroblast cells in the face of the scaffolding mentioned in 24 and 72 h was calculated based on the two-way ANOVA test and reported based on the statistical criterion P Hashemi and al., 2020 (figure 6). Using two-way ANOVA in MTT assays helps draw meaningful conclusions about how different treatments and time points affect cell growth, aiding in the understanding of cell viability and proliferation under various experimental conditions.

4.2 Cell life study by coloring DAPI

The DAPI colorology test was conducted for 24 h with three repetitions, and the data showed that the number of healthy nuclei in the scaffolding containing four substances was superior to the rest Hashemi and al., 2020 (Figs. 7 and 8).

* *PLA.PCL.HA:* Average 299.0 with a standard deviation of 66.57
* *PLA.PCL.Clay30B:* Average 303.0 with a standard deviation of 67.51
* *PLA.PCL.Clay30B.HA:* Average 356.7 with a standard deviation of 81.45

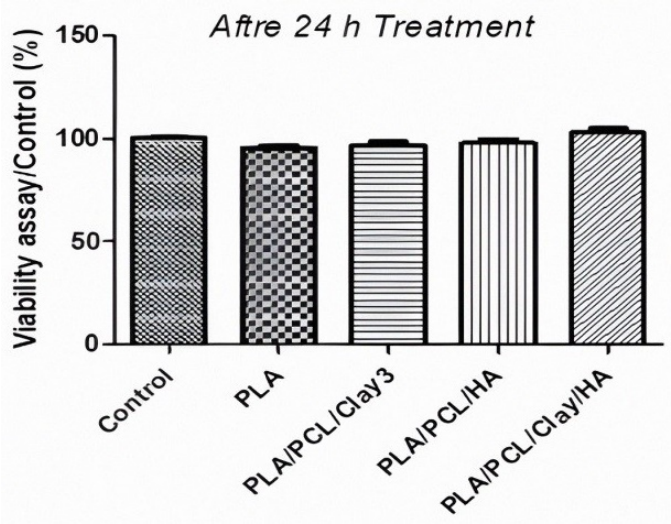

Figure 5. Cellular survival and cellular adaptation of PLA scaffolding, PLA/PCL/Clay30B, PLA/PCL/HA, PLA/PCL/Clay30B/HA.

The scaffold PLA.PCL.Clay.HA shows the highest average cell population (356.7), while the other two scaffolds have similar, slightly lower averages. The standard deviations indicate that the data dispersion in all three groups is approximately within the same range, with a slightly higher value for PLA.PCL.Clay.HA.

According to the *one-way analysis of variance (ANOVA): P value = 0.5800:* since the P-value is greater than 0.05 ($0.5800 > 0.05$), this means there is no significant difference in the average cell population among these three types of scaffolds overall.

On the graph, there are no stars next to the numbers or above the columns, which generally indicates that there are no statistically significant differences (at the usual significance level of 0.05) between the compared groups.

The absence of statistically significant differences in cell population among these three groups in the current DAPI test does not imply that there are no differences in other properties or long-term performance, nor does it mean that the current composition is the "best." It simply states that under the conditions of this experiment, with this criterion (DAPI staining) and this sample size, no noticeable differences were observed.

Ensuring the "most suitable" composition means we must consider all criteria relevant to the final application of the scaffold (e.g., tissue repair for bone, skin, etc.) and design and conduct specific experiments for each.

The MTT method measures cell viability based on metabolic activity and color production, while DAPI is used to assess cell count and viability through nuclear staining. Presenting these two methods separately is because each provides different information about the status of the cells, and together they can lend greater credibility to the results.

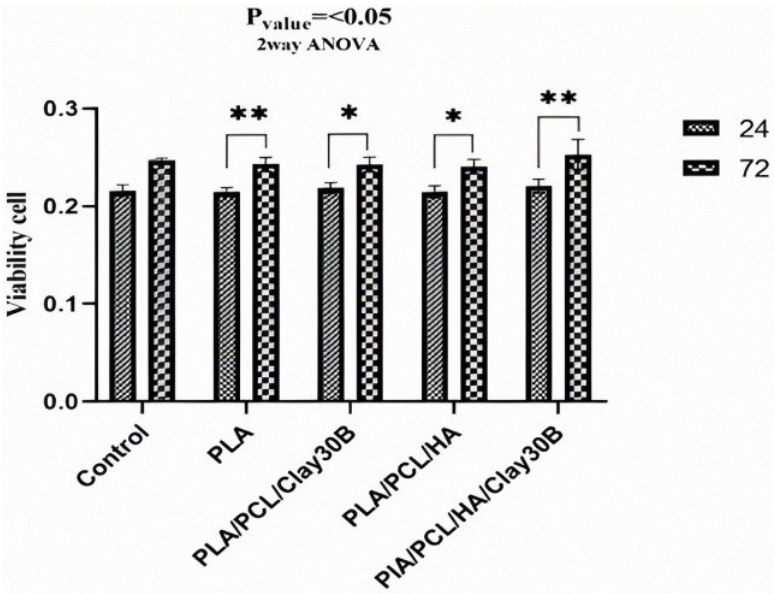

Figure 6. 24-h and 72-h the comparison of the MTT test on skin fibroblast.

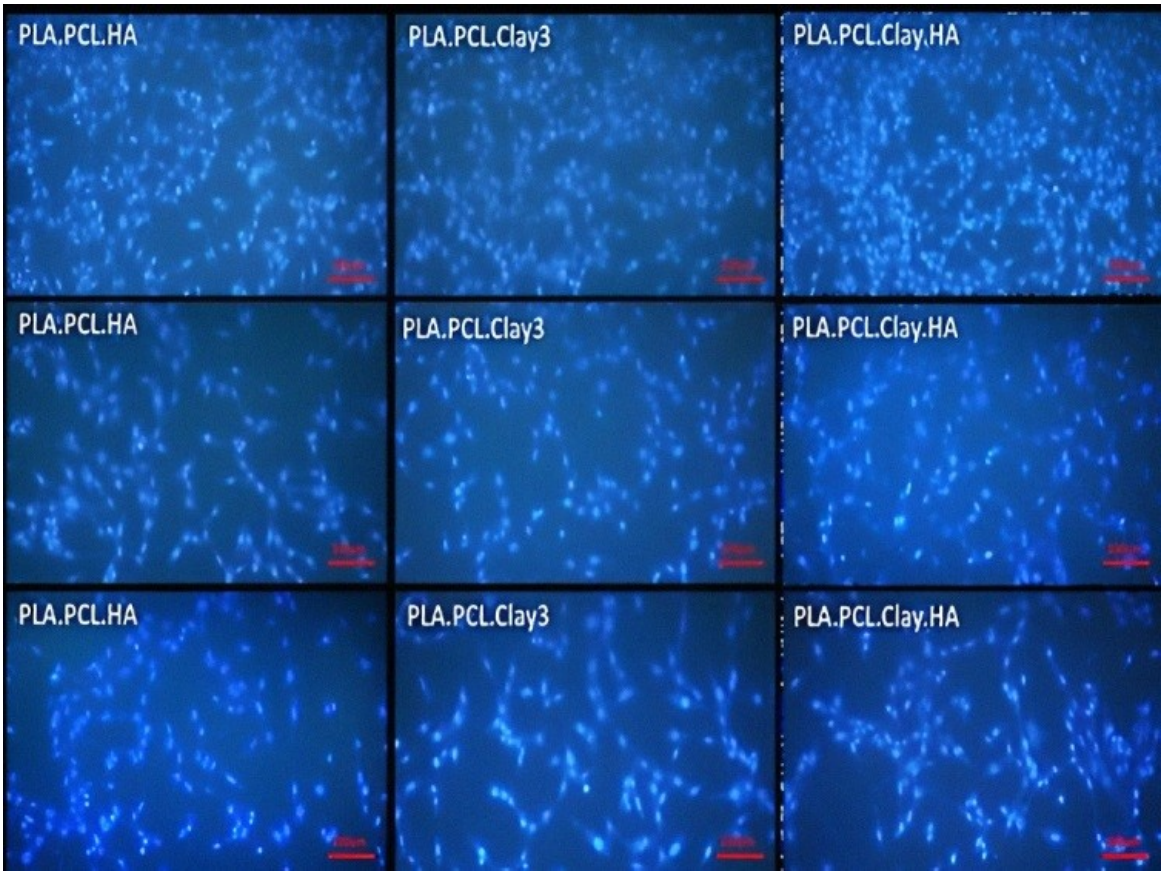

Figure 7. The analysis of the DAPI color data.

5. Conclusion

PLA/PCL/HA/Clay 30B composite scaffolding with the salting process, involving casting solvents, molding, and washing the porous substance, is intended to treat foot bone problems. The present study found that the proper diffusion of clay 30B and hydroxyapatite exists in the structure of PCL-PLA. It was observed that in the composite sample containing all four substances (PLA, PCL, clay 30B, and HA), the corresponding peaks of all four structures appeared, indicating successful compositing in this sample. Moreover, it was noted that in the sample containing all four compounds, the volume, number, and size of the holes grew larger and reached their highest value. This shows that the composition of all four materials creates a completely porous structure, which can benefit the final properties of the production scaffolding. In this composite, it was also observed that all the elements were distributed optimally throughout the material, indicating the proper distribution of hydroxyapatite and clay 30B in PLA/PCL composites. Furthermore, the composite had relatively high cell binding and proliferation and low cell toxicity.

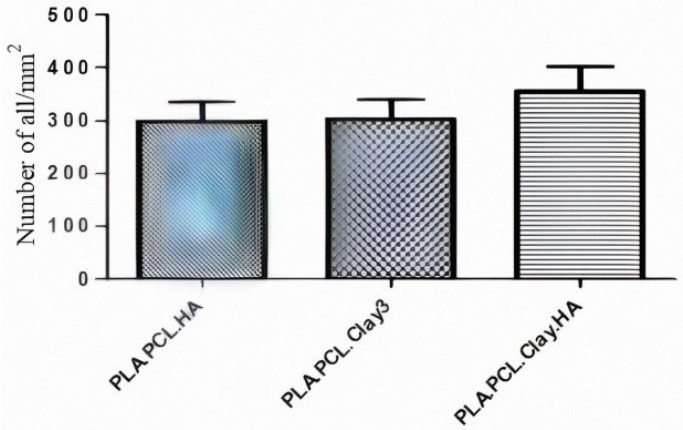

Figure 8. DAPI coloring.

Authors contributions
Authors have contributed equally in preparing and writing the manuscript.

Availability of data and materials
The data that support the findings of this study are available from the corresponding author, upon reasonable request.

Conflict of interests
The authors declare that they have no known competing financial interests or personal relationships that could have appeared to influence the work reported in this paper.

References

Abo-Elseoud W. S., Hassan M. L., Sabaa M. W., Basha M., Hassan E. A., Fadel S. M. (2018) Chitosan nanoparticles/cellulose nanocrystals nanocomposites as a carrier system for the controlled release of repaglinide. *Int. J. Biol. Macromol.* 111:604–613. DOI: https://doi.org/10.1016/j.ijbiomac.2018.01.055.

Ardekani-Zadeh A. H., Hosseini S. F. (2019) Electrospun essential oil-doped chitosan/poly (ε-caprolactone) hybrid nanofibrous mats for antimicrobial food biopackaging exploits. *Carbohydr. Polym.* 223:115108. DOI: https://doi.org/10.1016/j.carbpol.2019.115108.

Arunraj T. R., Sanoj Rejinold N., Kumar N. A., Jayakumar R. (2019) Corrigendum to "Bio-responsive chitin-poly(l-lactic acid) composite nanogels for liver cancer" [Colloids Surf. B 113 (2014) 394–402]. *Colloids Surf. B Biointerfaces* 181:76. DOI: https://doi.org/10.1016/j.colsurfb.2019.05.031.

Ayran M., Dirican A. Y., Saatcioglu E., Ulag S., Sahin A., Aksu B., al. et (2022) 3D-Printed PCL Scaffolds Combined with Juglone for Skin Tissue Engineering. *Bioengineering* 9 (8): 427. DOI: https://doi.org/10.3390/bioengineering9080427.

Choe H. C., Kim W. G., Jeong Y. H. (2010) Surface characteristics of HA coated Ti-30Ta-xZr and Ti-30Nb-xZr alloys after nanotube formation. *Surf. Coat. Technol.* 205:S305–S311. DOI: https://doi.org/10.1016/j.surfcoat.2010.08.058.

Choudhary R., Koppala S., Swamiappan S. (2015) Bioactivity studies of calcium magnesium silicate prepared from eggshell waste by sol–gel combustion synthesis. *J. Asian Ceram. Soc.* 3 (2): 173–177. DOI: https://doi.org/10.1016/j.jascer.2015.01.002.

Contri G., Zimmermann C. A., Ramoa S. D. A. D. S., Schmitz D. P., Ecco L. G., Barra G. M. de O., al. et (2020) Polypyrrole modified e-coat paint for corrosion protection of aluminum AA1200. *Front. Mater.* 7:45. DOI: https://doi.org/10.3389/fmats.2020.00045.

Evans S. K., Wesley O. N., Nathan O., Moloto M. J. (2019) Chemically purified cellulose and its nanocrystals from sugarcane baggase: isolation and characterization. *Heliyon* 5 (12): e02627. DOI: https://doi.org/10.1016/j.heliyon.2019.e02627.

Fil B. A., Özmetin C., Korkmaz M. (2014) Characterization and electrokinetic properties of montmorillonite. *J. Chem.* 2014:1–7. DOI: https://doi.org/10.1155/2014/483596.

Friné V. C., Hector A. P., Manuel N. D. S., Estrella N. D., Antonio G. J. (2019) Development and characterization of a biodegradable PLA food packaging hold Monoterpene–Cyclodextrin Complexes against Alternaria alternata. *Polymers* 11 (10): 1720. DOI: https://doi.org/10.3390/polym11101720.

Ghanbari M., Salavati-Niasari M., Mohandes F. (2021) Thermosensitive alginate–gelatin–nitrogen-doped carbon dots scaffolds as potential injectable hydrogels for cartilage tissue engineering applications. *RSC Adv.* 11 (30): 18423–18431. DOI: https://doi.org/10.1039/D1RA02835J.

Gokalp N., Ulker C., Avcibasi Guvenilir Y. (2016) Enzymatic ring opening polymerization Of É>-caprolactone by using a novel immobilized biocatalyst. *Adv. Mater. Lett.* 7 (2): 144–149. DOI: https://doi.org/10.5185/amlett.2016.6049.

Haider A., Haider S., Kummara M. R., Kamal T., Alghyamah A. A. A., Iftikhar F. J., al. et (2020) Advances in the scaffolds fabrication techniques using biocompatible polymers and their biomedical application: A technical and statistical review. *J. Saudi Chem. Soc.* 24 (2): 186–215. DOI: https://doi.org/10.1016/j.jscs.2020.01.002.

Hashemi S. S., al. et (2020) Polyurethane/chitosan/hyaluronic acid scaffolds: providing an optimum environment for fibroblast growth. *J. Wound Care* 29 (10): 586–596. DOI: https://doi.org/10.12968/jowc.2020.29.10.586.

Hassanajili S., Karami-Pour A., Oryan A., Talaei-Khozani T. (2019) Preparation and characterization of PLA/PCL/HA composite scaffolds using indirect 3D printing for bone tissue engineering. *Mater. Sci. Eng. C* 104:109960. DOI: https://doi.org/10.1016/j.msec.2019.109960.

Hsieh Y. T., Nozaki S., Kido M., Kamitani K., Kojio K., Takahara A. (2020) Crystal polymorphism of polylactide and its composites by X-ray diffraction study. *Polym. J.* 52 (7): 755–763. DOI: https://doi.org/10.1038/s41428-020-0343-8.

Islam M. M., al. et (2015) Preparation of gelatin based porous biocomposite for bone tissue engineering and evaluation of gamma irradiation effect on its properties. *Mater. Sci. Eng. C* 49:648–655. DOI: https://doi.org/10.1016/j.msec.2015.01.066.

Javid-Naderi M. J., Behravan J., Karimi-Hajishohreh N., Toosi S. (2023) Synthetic polymers as bone engineering scaffold. *Polym. Adv. Technol.* 34:2083–2096. DOI: https://doi.org/10.1002/pat.6049.

Jung M. R., Horgen F. D., Orski S. V., Rodriguez V., Beers K. L., Balazs G. H., al. et (2018) Validation of ATR FT-IR to identify polymers of plastic marine debris, including those ingested by marine organisms. *Mar. Pollut. Bull.* 127:704–716. DOI: https://doi.org/10.1016/j.marpolbul.2017.12.061.

Kareem M. M., Hodgkinson T., Sanchez M. S., Dalby M. J., Tanner K. E. (2019) Hybrid core–shell scaffolds for bone tissue engineering. *Biomed. Mater.* 14 (2): 025008. DOI: https://doi.org/10.1088/1748-605X/aafbf1.

Kundu K., Afshar A., Katti D. R., Edirisinghe M., Katti K. S. (2021) Composite nanoclay-hydroxyapatite-polymer fiber scaffolds for bone tissue engineering manufactured using pressurized gyration. *Compos. Sci. Technol.* 202:108598. DOI: https://doi.org/10.1016/j.compscitech.2020.108598.

Li D., Jiang Y., Lv S., Liu X., Gu J., Chen Q., al. et (2018) Preparation of plasticized poly (lactic acid) and its influence on the properties of composite materials. *PLoS One* 13 (5): e0193520. DOI: https://doi.org/10.1371/journal.pone.0193520.

Liu S., Zheng Y., Hu J., Wu Z., Chen H. (2020) Fabrication and characterization of polylactic acid/polycaprolactone composite macroporous micro-nanofiber scaffolds by phase separation. *New J. Chem.* 44 (41): 17382–17390. DOI: https://doi.org/10.1039/D0NJ03176C.

Luyt A. S., Gasmi S. (2016) Influence of blending and blend morphology on the thermal properties and crystallization behaviour of PLA and PCL in PLA/PCL blends. *J. Mater. Sci.* 51 (9): 4670–4681. DOI: https://doi.org/10.1007/s10853-016-9784-z.

Mohan S., Kumar V., Singh D. K., Hasan S. H. (2017) Effective removal of lead ions using graphene oxide-MgO nanohybrid from aqueous solution: isotherm, kinetic and thermodynamic modeling of adsorption. *J. Environ. Chem. Eng.* 5 (3): 2259–2273. DOI: https://doi.org/10.1016/j.jece.2017.04.031.

Mtavangu S. G., Mahene W., Machunda R. L., Bruggen B. van der, Njau K. N. (2022) Cockle (Anadara granosa) shells-based hydroxyapatite and its potential for defluoridation of drinking water. *Results Eng.* 13:100379. DOI: https://doi.org/10.1016/j.rineng.2022.100379.

Murugesan S., Scheibel T. (2020) Copolymer/clay nanocomposites for biomedical applications. *Adv. Funct. Mater.* 30 (40): 1908101. DOI: https://doi.org/10.1002/adfm.201908101.

Nandiyanto A. B. D., Oktiani R., Ragadhita R. (2019) How to read and interpret FTIR spectroscope of organic material. *Indones. J. Sci. Technol.* 4 (1): 97–118. DOI: https://doi.org/10.17509/ijost.v4i1.15806.

Nasrin R., Biswas S., Rashid T. U., Afrin S., Jahan R. A., Haque P., al. et (2017) Preparation of Chitin-PLA laminated composite for implantable application. *Bioact. Mater.* 2 (4): 199–207. DOI: https://doi.org/10.1016/j.bioactmat.2017.09.003.

Nga N. K., Huyen T. T. T., Dung T. N. (2023) Solvent casting-particulate leaching synthesis of a nano-SiO2/chitosan composite scaffold for potential use in bone tissue engineering. *Vietnam J. Chem.* 61 (S2): 1–9. DOI: https://doi.org/10.1002/vjch.202300080.

Park J. H., Lee B. K., Park S. H., Kim M. G., Lee J. W., Lee H. Y., al. et (2017) Preparation of biodegradable and elastic poly (ε-caprolactone-co-lactide) copolymers and evaluation as a localized and sustained drug delivery carrier. *Int. J. Mol. Sci.* 18 (3): 671. DOI: https://doi.org/10.3390/ijms18030671.

Perumal G., Pappuru S., Chakraborty D., Nandkumar A. M., Chand D. K., Doble M. (2017) Synthesis and characterization of curcumin loaded PLA—Hyperbranched polyglycerol electrospun blend for wound dressing applications. *Mater. Sci. Eng. C* 76:1196–1204. DOI: https://doi.org/10.1016/j.msec.2017.03.142.

Roshanghias A., Sodeifian G., Javidparvar A. A., Tarashi S. (2022) Construction of a novel polytetrafluoroethylene-based sealant paste: The effect of polyvinyl butyral (PVB) and nano-alumina on the sealing performance and construction formulations. *Results Eng.* 14:100460. DOI: https://doi.org/10.1016/j.rineng.2022.100460.

Solechan S., Suprihanto A., Widyanto S., Triyono J., Fitriyana D. F., Siregar J. P., al. et (2022) Investigating the Effect of PCL Concentrations on the Characterization of PLA Polymeric Blends for Biomaterial Applications. *Materials* 15 (20): 7396. DOI: https://doi.org/10.3390/ma15207396.

Somderama S., Aziza A. S. A., Abdullaha A. H., Matb R. (2019) Characterisation of NaA zeolite made from Malaysian Kaolin. *Chem. Eng. Trans.* 72:307–312. DOI: https://doi.org/10.3303/CET1972052.

Sri Aprilia N. A., Chintia Ambarita A., Karmila K., Adam Armando M., Yusupi Guswara F. (2017) Isolation and Characterization of Cellulose Nanofiber (CNF) from Sugarcane Bagasse by Acid Hydrolysis with Addition of Ferric Chloride Catalyst (FeCl3). *Orient. J. Phys. Sci.* 2 (2): 103–108. DOI: https://doi.org/10.13005/OJPS02.02.04.

Sun H., Yu B., Han J., Kong J., Meng L., Zhu F. (2014) Microstructure, thermal properties and rheological behavior of PLA/PCL blends for melt-blown nonwovens. *Polymer* 38 (4): 477–483. DOI: https://doi.org/10.1016/j.polymer.2014.02.018.

Tang C. M., Tian Y. H., Hsu S. H. (2015) Poly (vinyl alcohol) nanocomposites reinforced with bamboo charcoal nanoparticles: Mineralization behavior and characterization. *Materials* 8 (8): 4895–4911. DOI: https://doi.org/10.3390/ma8084895.

Torre G. Carbajal-De la, Zurita-Méndez N. N., Ballesteros-Almanza M. L., Mendoza K., Espinosa-Medina M. A., Ortiz-Ortiz J. (2021) Synthesis and characterization of polylactic / polycaprolactone / hydroxyapatite (PLA/PCL/HAp) scaffolds. *MRS Adv.* 6 (34): 903–906. DOI: https://doi.org/10.1557/s43580-021-00136-8.

Wang S., Meng X., Liu N., Shi L. (2022) Alkylation for removing trace olefins from reforming aromatics over novel Al2O3@SO42-/ZrO2 catalysts derived from the ZrO2-coated γ-Al2O3 strategy. *Sep. Purif. Technol.* 308:122731. DOI: https://doi.org/10.1016/j.seppur.2022.122731.

Yao Q., Cosme J. G. L., Xu T., Miszuk J. M., Picciani P. H. S., Fong H., al. et (2017) Three dimensional electrospun PCL/PLA blend nanofibrous scaffolds with significantly improved stem cells osteogenic differentiation and cranial bone formation. *Biomaterials* 115:115–127. DOI: https://doi.org/10.1016/j.biomaterials.2016.11.018.